iScience

CellPress
OPEN ACCESS

Article

Simulated spaceflight-induced cardiac remodeling is modulated by gut microbial-derived trimethylamine N-oxide

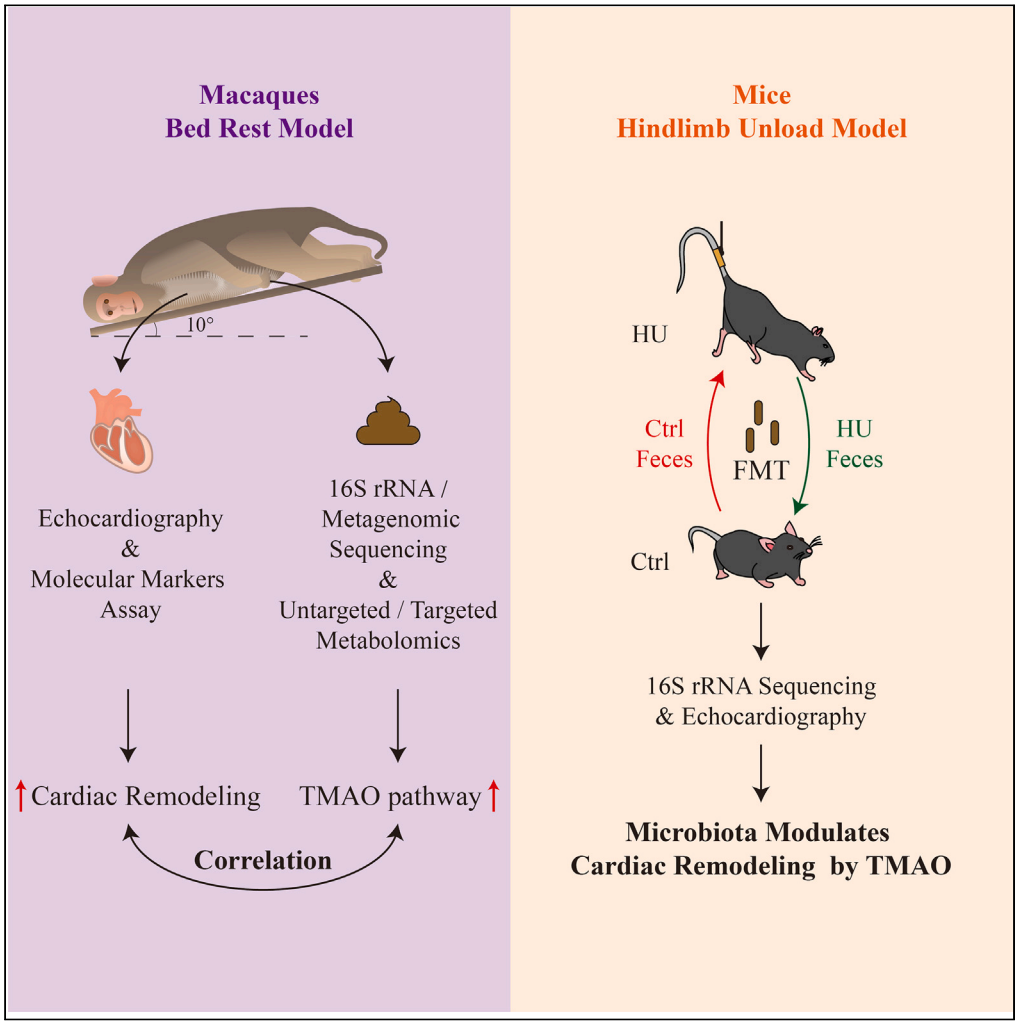

Zizhong Liu, Gui Luo, Ruikai Du, ..., Huiyuan Sun, Shukuan Ling, Yingxian Li

liuzizhong911@163.com (Z.L.)
sh2ling@126.com (S.L.)
yingxianli@aliyun.com (Y.L.)

Highlights

Cardiac remodeling correlated with TMAO in HDBR macaques

Cardiac remodeling modulated by gut microbiota, which correlated with TMAO in HU mice

Simulated spaceflight-induced cardiac remodeling modulated by the gut microbiota

Liu et al., iScience 26, 108556
December 15, 2023 © 2023
https://doi.org/10.1016/j.isci.2023.108556

iScience

CellPress
OPEN ACCESS

Article

Simulated spaceflight-induced cardiac remodeling is modulated by gut microbial-derived trimethylamine N-oxide

Zizhong Liu,[1,8,9,*] Gui Luo,[2,8] Ruikai Du,[1] Guanghan Kan,[1] Xuan Han,[1] Guohui Zhong,[1] Wenjuan Xing,[3] Ying Cui,[4] Weijia Sun,[1] Jianwei Li,[1] Yuheng Li,[1] Dingsheng Zhao,[1] Xinxin Yuan,[1] Xiaoyan Jin,[1] Yanping Han,[5] Huiyuan Sun,[6] Shukuan Ling,[7,*] and Yingxian Li[1,*]

SUMMARY

Spaceflight is physically demanding and can negatively affect astronauts' health. It has been shown that the human gut microbiota and cardiac function are affected by spaceflight and simulated spaceflight. This study investigated the effects of the gut microbiota on simulated spaceflight-induced cardiac remodeling using 10° of head-down bed rest (HDBR) in rhesus macaques and 30° of hindlimb unloading (HU) in mice. The gut microbiota, fecal metabolites, and cardiac remodeling were markedly affected by HDBR in macaques and HU in mice, cardiac remodeling in control mice was affected by the gut microbiota of HU mice and that of HU mice was protected by the gut microbiota of control mice, and there was a correlation between cardiac remodeling and the gut microbial-derived metabolite trimethylamine N-oxide. These findings suggest that spaceflight can affect cardiac remodeling by modulating the gut microbiota and fecal metabolites.

INTRODUCTION

Space is a harsh environment in which profound changes in the physiology of astronauts may negatively affect the entire spaceflight mission.[1,2] The gut microbiota is sensitive to endogenous and environmental factors, and specific human experiences and environmental conditions can have a marked effect on this microbial community.[3,4] Previous studies showed that the composition and function of the human gut microbiota was affected by spaceflight.[5,6] The diverse microbial community that comprises the human gut microbiota is increasingly recognized as playing an important role in human physiology, including cardiac remodeling.[7,8] The gut microbiota also has an important role in human health by producing short-chain fatty acids (SCFAs), vitamins, amino acids, and gut microbial-derived trimethylamine N-oxide (TMAO); training the immune system; protecting against pathogens; and contributing to the maturation of the intestinal epithelium.[9–13] TMAO is a metabolite that is converted from trimethylamine via flavin-containing monooxygenases in the liver, and trimethylamine is formed from dietary phosphatidylcholine via the gut microbiota.[11] There have been several reports suggesting that circulating TMAO is a deleterious end product and associated with heart failure and cardiovascular disease.[7,11,14,15] Moreover, in the harsh environment of space, the human cardiovascular system undergoes various changes, and cardiac remodeling is associated with a decline in cardiac function.[16,17] However, no study has investigated the effect of true or simulated spaceflight on cardiac remodeling by the gut microbiota.

In view of the limited opportunities for true spaceflight, head-down bed rest (HDBR) and hindlimb unloading (HU) have been used as simulation models to recreate the specific environmental factors of confinement, stress, and altered physical conditions of microgravity when researching the physiological effects of spaceflight.[18–20] A number of studies have demonstrated that spaceflight, HDBR, and HU affect the immune, cardiovascular, and musculoskeletal systems and the gut microbiota.[21–24] However, the relationship between the gut microbiota and physiology during spaceflight is not well understood in humans.

This study explored the effects of the gut microbiota on simulated spaceflight-induced cardiac remodeling in rhesus macaques exposed to HDBR and mice exposed to HU. First, fecal samples from macaques were analyzed by 16S rRNA gene sequencing, metagenomic sequencing,

[1]National Key Laboratory of Space Medicine, China Astronaut Research and Training Center, Beijing, China
[2]Department of Rheumatology and Immunology, First Medical Center of Chinese PLA General Hospital, Beijing, China
[3]School of Aerospace Medicine, Key Laboratory of Aerospace Medicine of the Ministry of Education, Fourth Military Medical University, Xi'an, China
[4]School of Traditional Chinese Medicine, Beijing University of Chinese Medicine, Beijing, China
[5]State Key Laboratory of Pathogen and Biosecurity, Beijing Institute of Microbiology and Epidemiology, Beijing, China
[6]Beijing University of Chinese Medicine Third Affiliated Hospital, Beijing, China
[7]Oujiang Laboratory, Zhejiang Lab for Regenerative Medicine, Vision and Brain Health, Wenzhou, Zhejiang, China
[8]These authors contributed equally
[9]Lead contact
*Correspondence: liuzizhong911@163.com (Z.L.), sh2ling@126.com (S.L.), yingxianli@aliyun.com (Y.L.)
https://doi.org/10.1016/j.isci.2023.108556

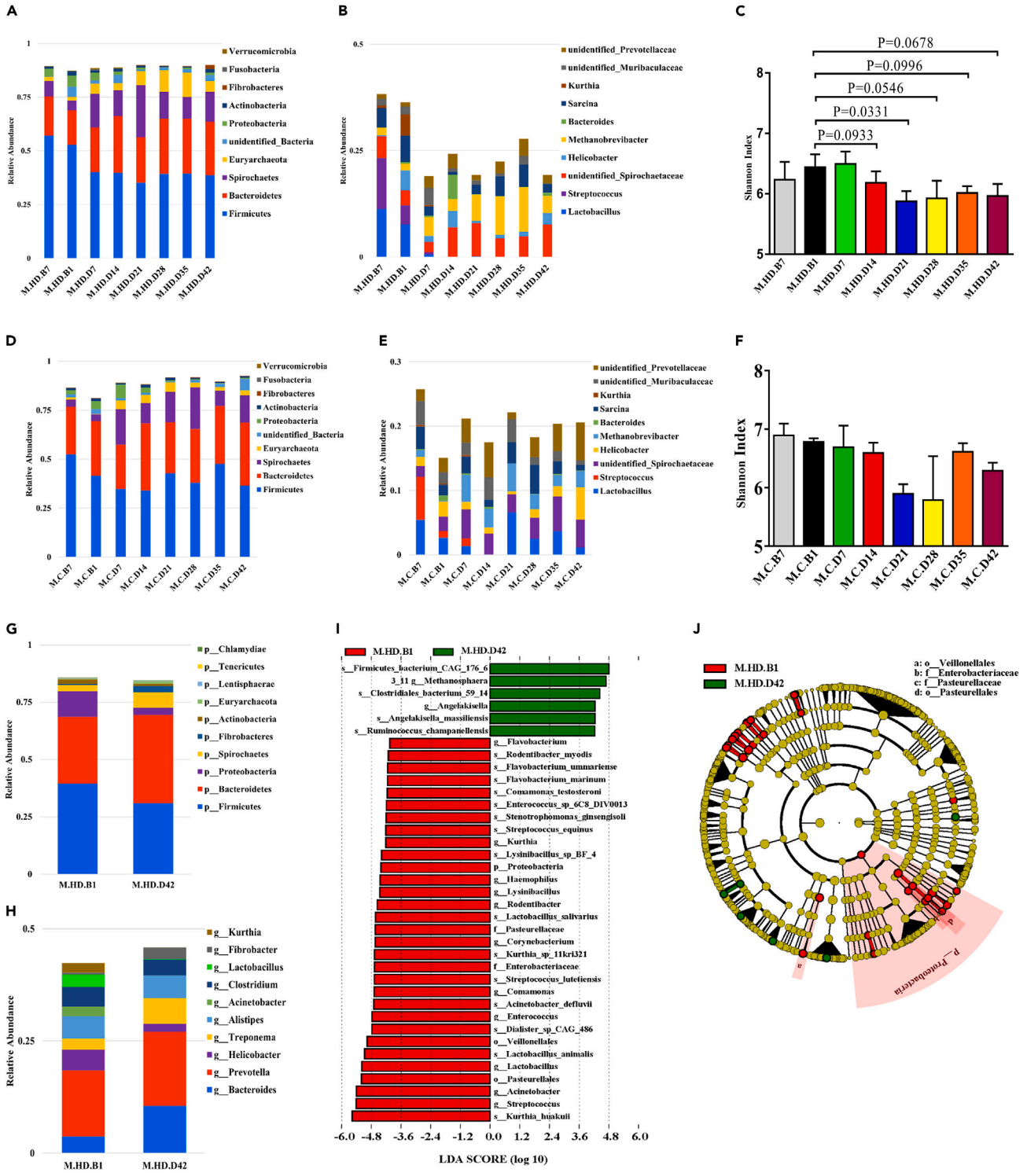

Figure 1. Fluctuations in gut microbiota in HDBR and control rhesus macaques

(A) Top ten phylum abundances in gut microbiota of HDBR rhesus macaques at eight time points by 16S rRNA gene sequencing.

(B) Top ten genus abundances in gut microbiota of HDBR rhesus macaques at eight time points by 16S rRNA gene sequencing.

(C) Comparison of α-diversity across eight time points in HDBR rhesus macaques by 16S rRNA gene sequencing.

(D) Top ten phylum abundances in gut microbiota of control rhesus macaques at eight time points by 16S rRNA gene sequencing.

(E) Top ten genus abundances in gut microbiota of control rhesus macaques at eight time points by 16S rRNA gene sequencing.

Figure 1. *Continued*

(F) Comparison of α-diversity across eight time points in control rhesus macaques by 16S rRNA gene sequencing.

(G) Top ten phylum abundances in gut microbiota before and after HDBR by metagenomic sequencing.

(H) Top ten genus abundances in gut microbiota before and after HDBR by metagenomic sequencing.

(I) Diagram showing the distribution of LDA scores and results of the LEfSe analysis based on the LDA score to screen for species biomarkers. LDA scores for the above four species between M.HD.B1 and M.HD.D42 differed significantly.

(J) Cladogram based on different species. Red and green nodes represent the microorganisms that played an important role in each group. Abbreviation: one week before HDBR in macaques (M.HD.B7), one day before HDBR in macaques (M.HD.B1), one week during HDBR in macaques (M.HD.D7), two weeks during HDBR in macaques (M.HD.D14), three weeks during HDBR in macaques (M.HD.D21), four weeks during HDBR in macaques (M.HD.D28), five weeks during HDBR in macaques (M.HD.D35), six weeks during HDBR in macaques (M.HD.D42).

and untargeted and targeted metabolomics. Next, cardiac remodeling in the macaques was analyzed by transthoracic echocardiography and quantitative real-time PCR assays. We found that the gut microbiota, fecal metabolites, and cardiac remodeling were markedly affected by HDBR and that cardiac remodeling was correlated with gut microbial-derived TMAO. Fecal microbiota transplantation (FMT) was used to demonstrate the effect of the gut microbiota on cardiac remodeling in the HU mouse model, and the gut microbial-derived TMAO was correlated with cardiac remodeling. This study is the first to elucidate the impact of simulated spaceflight on cardiac remodeling by the gut microbiota, and its results are critical for research into how changes in the gut microbiota affect human physiology and psychology under spaceflight conditions. Its findings also provide insights regarding how to maintain an astronaut's gut microbiota during spaceflight, which is critical in terms of avoiding adverse effects and ensuring the success of the spaceflight mission.

RESULTS

HDBR had a marked effect on the gut microbiota in macaques

The gut microbiotas of six HDBR macaques and three control macaques were tracked over eight time points. Fecal samples were collected and characterized by 16S rRNA gene sequencing and metagenomic sequencing. First, we characterized the composition of the gut microbiota in the macaques by 16S rRNA gene sequencing. After HDBR, the gut microbiota fluctuated markedly at both the phylum and genus levels. Fluctuations in the top 10 most abundant microorganisms in the gut microbiota at the phylum level are shown in Figure 1A. The abundance of Firmicutes decreased markedly after HDBR. Bacteroidetes and Spirochaetes increased markedly in abundance after HDBR. Fluctuations in the top 10 most abundant microbes in the gut microbiota at the genus level are shown in Figure 1B. There was a marked decrease in the abundances of *Lactobacillus* and *Streptococcus* after HDBR. The abundance of *Methanobrevibacter* increased markedly after HDBR. The α-diversity of each sample was estimated using the Shannon index based on the genus profile and was found to be decreased after HDBR (Figure 1C). However, there was no markedly change in the top 10 most abundant microorganisms in the gut microbiota at the phylum or genus level or in the α-diversity at the genus level in the control macaques (Figures 1D–1F). Furthermore, 16S rRNA gene sequencing showed that HDBR had a marked effect on the abundance of organisms in the gut microbiota at other classification levels (class, order, family, and species; Figure S1). We then characterized the gut microbiotas of six HDBR macaques at the B1 (one day before HDBR) and D42 (6 weeks during HDBR) time points by metagenomic sequencing to investigate how HDBR affects the composition and function of the gut microbiota in macaques in more detail. Consistent with the results of 16S rRNA gene sequencing, the gut microbiotas showed clear fluctuations after HDBR at both the phylum and genus levels. Fluctuations in the top 10 most abundant microorganisms in the gut microbiota at the phylum level are shown in Figure 1G. After HDBR, there were marked decreases in the abundances of Firmicutes and Proteobacteria and marked increases in the abundances of Bacteroidetes and Spirochaetes. We also found fluctuations in the top 10 most abundant microbes in the gut microbiota at the genus level (Figure 1H). *Lactobacillus*, *Acinetobacter*, and *Helicobacter* showed marked decreases and *Bacteroides* and *Treponema* showed marked increases in abundance after HDBR. Metagenomic sequencing also revealed that HDBR had a marked effect on abundances in the gut microbiota at other levels (class, order, family, and species; Figure S2). To explore the differences among species in the gut microbiota of the macaque that were affected by HDBR, we performeda linear discriminant analysis (LDA) effect size analysis to identify species biomarkers. We compared the composition of the gut microbiota at the B1 and D42 time points, displayed the LDA species score, and constructed a distribution diagram of differences in species at all levels and a cladogram based on the different species (Figure 1I, Table S1). After HDBR, there was a decrease in abundance of 31 species and an increase in abundance of six species at all levels. The cladogram based on the different species is shown in Figure 1J. To investigate how HDBR affects the function of the gut microbiota in macaques, we blasted unigenes against the KEGG, eggNOG, and CAZy databases and identified the relative abundances of these sequences in the KEGG (Figure S3A), eggNOG (Figure S3B), and CAZy (Figure S3C) databases at level 1. We found that HDBR markedly affected the function of the gut microbiota, especially the relative abundance of metabolism genes in KEGG level 1 and that of glycoside hydrolase genes in CAZy level 1.

Fecal metabolites in macaques were markedly affected by HDBR and correlated with fluctuations in the gut microbiota

The effect of HDBR on the gut microbial-derived metabolites was investigated in macaques using untargeted and targeted metabolomics. First, we showed the different fecal metabolites of macaques before and after HDBR in a volcano plot for positive polarity mode (Figure 2A). In positive polarity mode, there were 248 fecal metabolites, the abundance of which was increased in 134 and decreased in 114 after HDBR (Table S2). The clustering heatmap and principal component analysis (PCA) plot of these fecal metabolites are shown in Figures S4A and S4C. When the fecal metabolites were subjected to metabolic pathway enrichment analysis by KEGG (Figure 2B), the pathways of pyrimidine and purine metabolism were found to be markedly affected by HDBR. In negative polarity mode, the different fecal metabolites of macaques

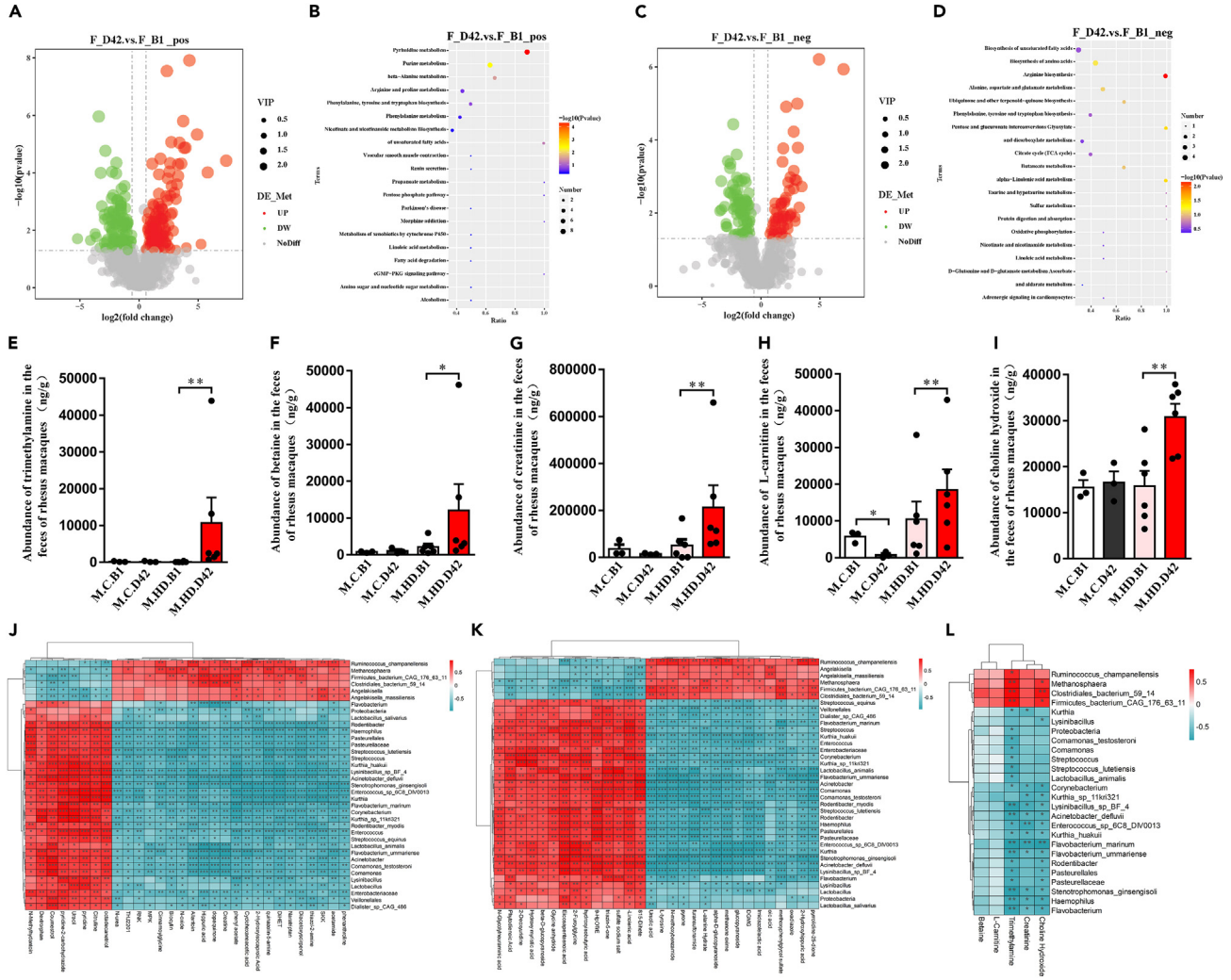

Figure 2. Fluctuations in fecal metabolites in HDBR rhesus macaques and the correlation between metabolites and the gut microbiota

(A) Volcano plot of fecal metabolites before and after HDBR for the positive polarity mode. Metabolites with a variable importance in projection value > 1, a p-value <0.05, and a fold change ≥2 or ≤0.5 were considered to be differential metabolites.

(B) Metabolic pathway enrichment analysis of differential metabolites performed by KEGG for the positive polarity mode.

(C) Volcano plot showing fecal metabolites in macaques before and after HDBR for the negative polarity mode.

(D) Metabolic pathway enrichment analysis of differential metabolites performed by KEGG for the negative polarity mode.

(E–I) Concentrations of gut microbial TMAO pathway metabolites in control and HDBR macaques by targeted metabolomics, including trimethylamine (E), betaine (F), creatinine (G), L-carnitine (H), and choline hydroxide (I).

(J) Correlation between the top 30 differential metabolites for the positive polarity mode and differential species biomarkers.

(K) Correlation between the top 30 differential metabolites for the negative polarity mode and differential species biomarkers.

(L) Correlation between gut microbial TMAO pathway metabolites and differential species biomarkers.

*p < 0.05, **p < 0.01, and ***p < 0.001.

before and after HDBR were showed in a volcano plot (Figure 2C); there were 143 fecal metabolites, the abundance of which was increased in 64 and decreased in 79 after HDBR (Table S3). The clustering heatmap and PCA plot of these metabolites are shown in Figures S4B and S4D. When the fecal metabolites were subjected to metabolic pathway enrichment analysis by KEGG (Figure 2D), the pathways for biosynthesis of arginine and amino acids were markedly affected by HDBR. From other studies, we found that the abundances of SCFAs, bile acids, and the gut microbial TMAO pathway were correlated with cardiac dysfunction, so the abundances of SCFAs and bile acids in the gut microbial TMAO pathway were then analyzed by targeted metabolomics. We found significant increases in the abundance of several metabolites, particularly in trimethylamine but also in betaine, creatinine, L-carnitine, and choline hydroxide, in the gut microbial TMAO pathway in HDBR macaques but no significant changes in these metabolites in control macaques (Figures 2E–2I). Furthermore, there was no significant difference in the abundance of gut microbial SCFAs (Figure S5) or bile acids (Figure S6) in either the HDBR or control macaques before or after HDBR. The

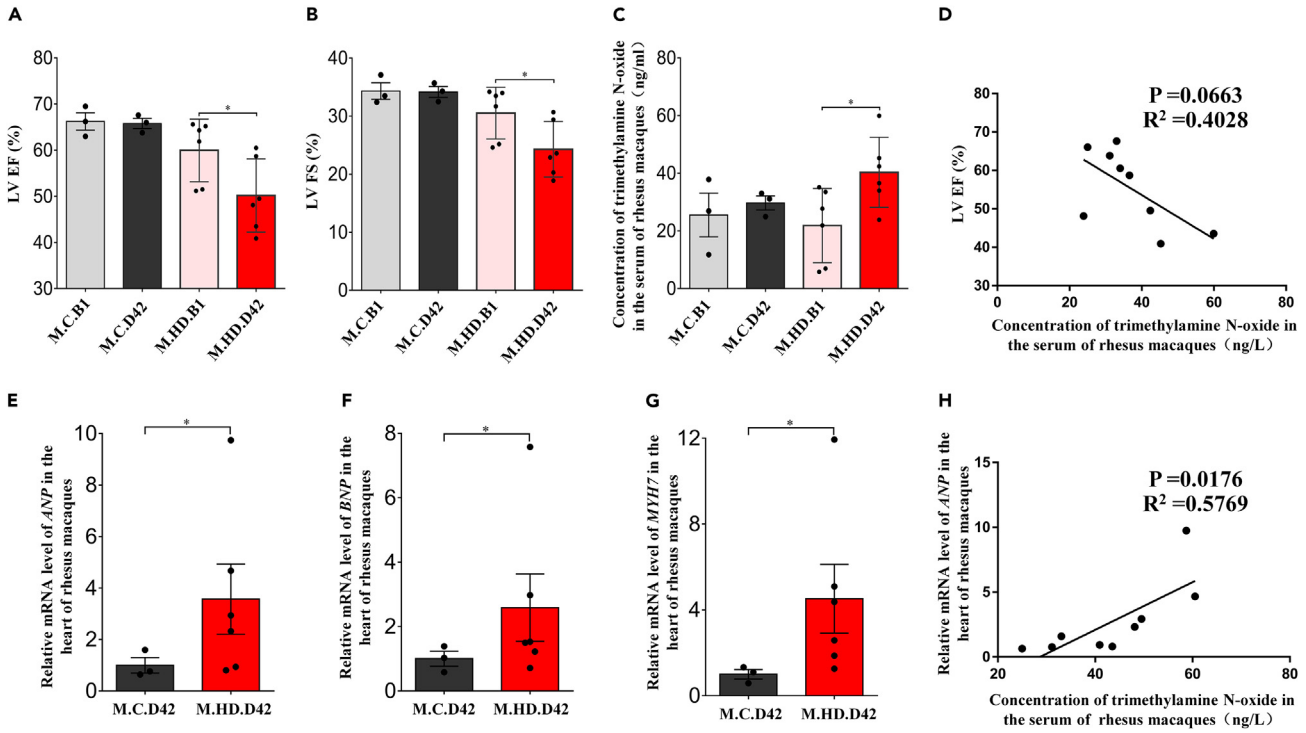

Figure 3. Cardiac remodeling in rhesus macaques was influenced by HDBR and correlated with serum TMAO

(A and B) Echocardiograms showing the LVEF and LVFS in the control and HDBR macaques.

(C) The serum TMAO concentration was measured by enzyme-linked immunosorbent assay.

(D) Correlation of LVEF with the serum TMAO level.

(E–G) Relative mRNA levels of *ANP*, *BNP*, and *MYH7* in the heart were analyzed by quantitative polymerase chain reaction assay.

(H) Correlation of the relative mRNA level of *ANP* in the heart with the serum TMAO concentration.

*p < 0.05, **p < 0.01, and ***p < 0.001.

correlations between the differential species biomarkers identified by metagenomic sequencing and the top 30 differential metabolites identified by untargeted metabolomics in positive and negative polarity modes are shown in Figures 2J and 2K, respectively. In the heatmap, almost all of the differential species biomarkers showed a positive or negative correlation with the differential metabolites. We also found a correlation between the differential species biomarkers and the abundance of metabolites in the gut microbial TMAO pathway (Figure 2L). In the heatmap, the differential species biomarkers showed positive or negative correlations with trimethylamine, creatinine, and choline hydroxide. The effect of HDBR on serum metabolites in macaques was then explored by untargeted metabolomics. The different metabolites before and after HDBR are shown by volcano plots for positive and negative polarity modes in Figures S7A and S7C. Metabolic pathway enrichment analysis by KEGG showed that the pathways for metabolism of purines and biosynthesis of amino acids were markedly affected by HDBR (Figures S7B and S7D), which was consistent with the change in fecal metabolites.

Cardiac remodeling in macaques was affected by HDBR and correlated with gut microbial-derived TMAO

The effect of HDBR on cardiac remodeling was explored by monitoring structural and functional changes in the heart by echocardiography. After HDBR, there were significant decreases in left ventricular ejection fraction (LVEF) and left ventricular fractional shortening (LVFS); however, there was no significant change in either of these parameters in the control macaques (Figures 3A and 3B). The post-HDBR changes were accompanied by significant decreases in interventricular septal diameter and end-diastolic left ventricular posterior wall thickness (LVPWd) and a significant increase in end-systolic volume with no change in end-diastolic left ventricular internal diameter (LVIDd), end-systolic left ventricular internal diameter (LVIDs), or end-diastolic volume (Figure S8). The detailed cardiac parameters obtained from echocardiography were shown in Table S4. In view of the increased abundance of metabolites in the gut microbial TMAO pathway in the feces of HDBR macaques, we measured the serum TMAO concentration and found it to be increased in the HDBR macaques but not significantly changed in the control macaques (Figure 3C). We also found a negative correlation between the serum TMAO level and the LVEF in both HDBR and control macaques (Figure 3D). At the molecular level, markers of hypertrophy, including atrial natriuretic peptide (ANP), brain natriuretic peptide (BNP), and myosin heavy chain 7 (MYH7), were significantly upregulated in HDBR macaques but not in control macaques (Figures 3E–3G). The serum TMAO level was positively correlated with the relative mRNA level of *ANP* in the heart in both HDBR and control macaques (Figure 3H).

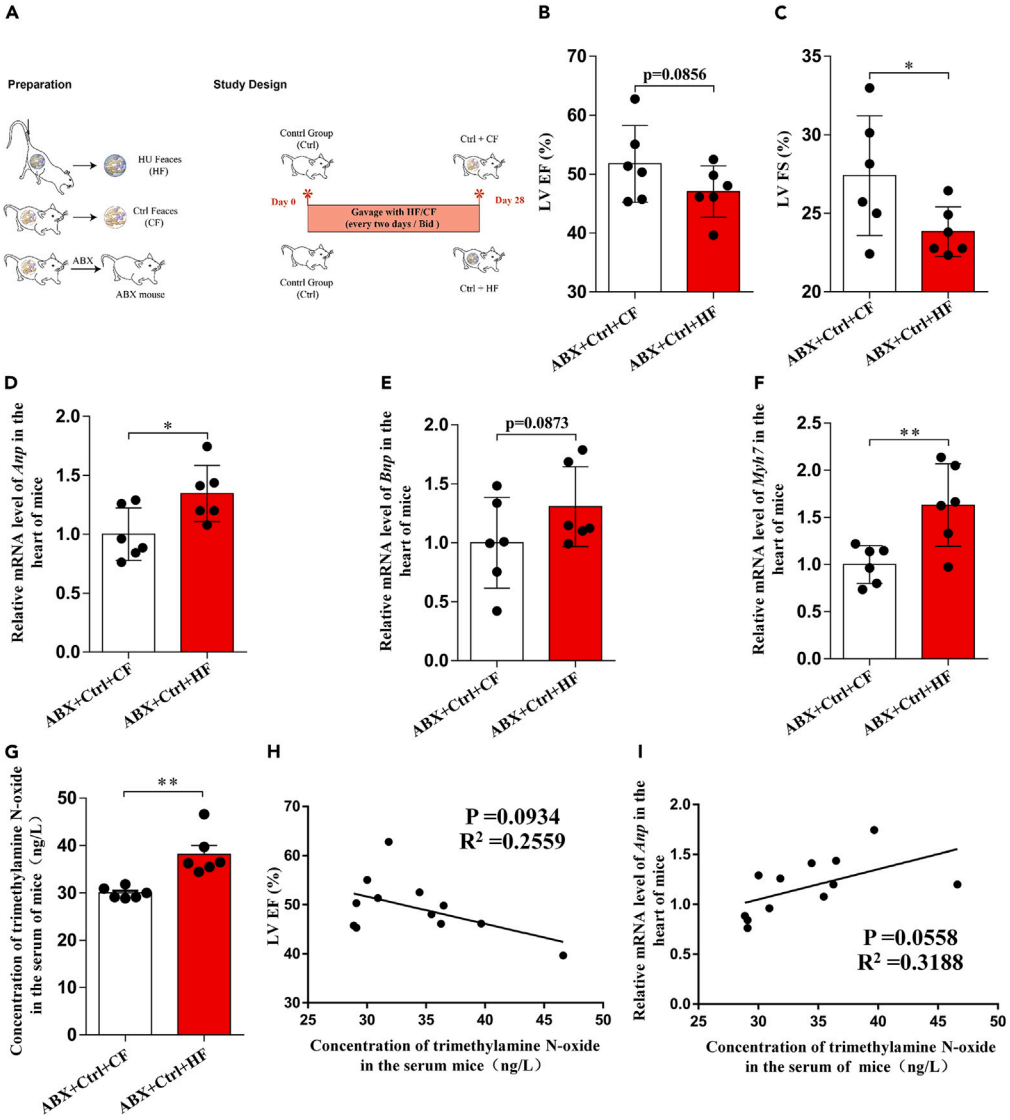

Figure 4. Cardiac remodeling in control mice was influenced by the gut microbiota of control and HU mice and correlated with serum TMAO

(A) Overview of the study design and protocol for fecal microbiota transplantation.

(B and C) Echocardiograms showing LVEF and LVFS.

(D–F) Relative mRNA levels of *ANP*, *BNP*, and *MYH7* in the heart were analyzed by quantitative polymerase chain reaction assay.

(G) The serum TMAO concentration was detected by enzyme-linked immunosorbent assay.

(H) Correlation of LVEF with the serum TMAO concentration.

(I) Correlation of the relative mRNA level of *ANP* in the heart with the serum TMAO concentration.

*p < 0.05, **p < 0.01, and ***p < 0.001.

The gut microbiota of HU mice induced cardiac remodeling in control mice and correlated with TMAO

The effect of the gut microbiota on cardiac remodeling induced by simulated spaceflight was explored by FMT, whereby the gut microbiota of control and HU mice were transplanted into antibiotic-treated control mice. The design of the FMT component of the study is shown in Figure 4A. The mice were monitored for structural and functional changes in the heart by echocardiography. We found markedly decreases in LVEF and LVFS in the mice that had been gavaged with the feces of HU mice (the HF group) in comparison with those that were gavaged with the feces of control mice (the CF group) (Figures 4B and 4C). There were no significant changes in end-diastolic and end-systolic left ventricular anterior wall thickness (LVAWd and LVAWs, respectively) in the CF group or the HF group (Figures S9A and S9B). However, in the HF group, there were significant decreases in end-diastolic and end-systolic left ventricular posterior wall thickness (LVPWd and LVPWs, respectively; Figures S9C and S9D) and significant increases in end-diastolic and end-systolic left ventricular internal diameter and

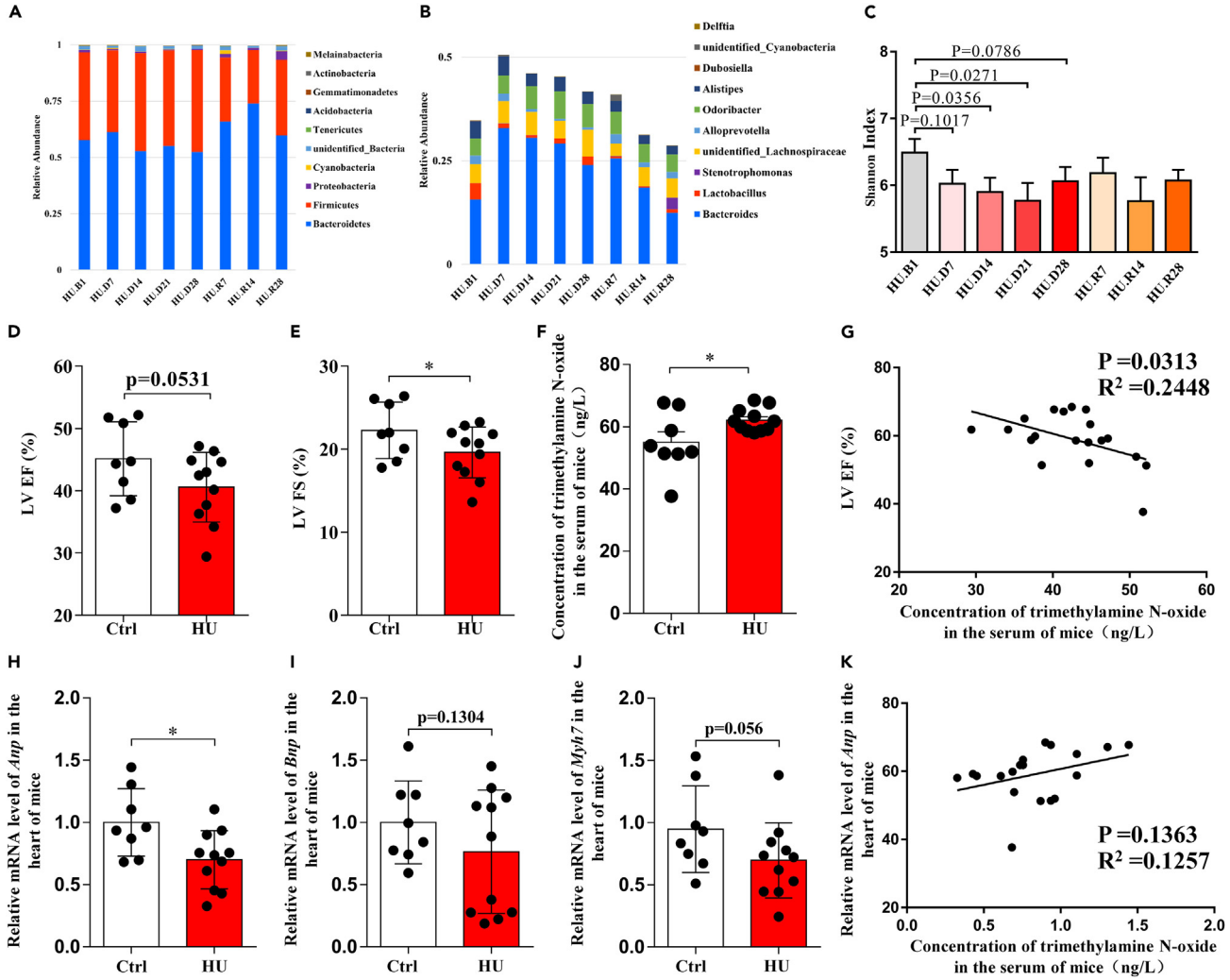

Figure 5. Influence of HU on the gut microbiota and cardiac remodeling in mice

(A) Top ten phylum abundances in gut microbiota at eight time points by 16S rRNA gene sequencing.

(B) Top ten genus abundances in gut microbiota at eight time points by 16S rRNA gene sequencing.

(C) Comparison of α-diversity across eight time points by 16S rRNA gene sequencing.

(D and E) Echocardiograms showing the LVEF and LVFS in control and HU mice.

(F) The serum TMAO concentration was detected by enzyme-linked immunosorbent assay.

(G) Correlation of LVEF with the serum TMAO concentration.

(H–J) Relative mRNA levels of *ANP*, *BNP*, and *MYH7* in the heart were analyzed by quantitative polymerase chain reaction assay.

(K) Correlation of the relative mRNA level of *ANP* in the heart with the serum TMAO concentration.

*p < 0.05, **p < 0.01, and ***p < 0.001.

volume (LVIDd, LVIDs, LVVold, and LVVols, respectively; Figures S9E–S9H). ANP, BNP, and MYH7 were significantly upregulated in the HF group but not in the CF group (Figures 4D–4F). The serum TMAO level was higher in the HF group than in the CF group (Figure 4G) and was negatively correlated with LVEF (Figure 4H). Furthermore, there was a positive correlation between the serum TMAO level and the relative mRNA level of *ANP* (Figure 4I).

The gut microbiota, fecal metabolites, and cardiac remodeling were markedly affected by HU in mice and cardiac remodeling was correlated with TMAO

The gut microbiotas of the HU and control mice were tracked at eight time points by collection of fecal samples and characterizing them by 16S rRNA gene sequencing. The gut microbiota showed fluctuations at both the phylum and genus levels after HU and varying degrees of recovery after 4 weeks without HU. The fluctuations in the top 10 most abundant microorganisms in the gut microbiota at the phylum level are shown in Figure 5A. The abundance of Firmicutes increased slightly and that of Bacteroidetes decreased slightly after HU and recovered

within 4 weeks of cessation of HU. Fluctuations in the top 10 most abundant microbes in the gut microbiota at the genus level are shown in Figure 5B. The abundance of *Bacteroides* was markedly increased and that of *Lactobacillus* was markedly decreased after HU. The α-diversity of each sample at the genus level was estimated using the Shannon index and found to be decreased after HU (Figure 5C). However, the top 10 most abundant microorganisms in the gut microbiota of the control mice showed no markedly change at the phylum or genus level or in α-diversity at the genus level (Figure S10). Furthermore, HU had a marked effect on the abundance of organisms in the gut microbiota at other classification levels (class, order, family, and species; Figure S11). The effect of HU on mouse gut microbial-derived metabolites was investigated using untargeted metabolomics. First, we constructed volcano plots for positive and negative polarity modes showing the different fecal metabolites in the mice before and after HU (Figures S12A and S12C). The fecal metabolites were then subjected to metabolic pathway enrichment analysis by KEGG (Figures S12B and S12D). The purine metabolism pathway was found to be affected by HU in both positive and negative polarity modes. Cardiac structure and function was monitored after HU by echocardiography. LVEF, LVFS, LVAWd, and LVPWs were found to be significantly decreased in the HU mice in comparison with the control mice (Figures 5D, 5E, and S13) whereas LVIDs was significantly increased in the HU mice with no significant change in LVAWs, LVPWd, LVIDd, LVVold, or LVVols (Figure S13). The serum TMAO level was higher in the HU mice than in the control mice (Figure 5F). There was also a negative correlation between the serum TMAO concentration and LVEF (Figure 5G). ANP was significantly upregulated; BNP and MYH7 were upregulated in the HU mice but not in the control mice (Figures 5H–5J). The serum TMAO concentration was positively correlated with the relative mRNA level of *ANP* (Figure 5K).

The gut microbiota in control mice protected against HU-induced cardiac remodeling and was correlated with TMAO

FMT was used to explore the ability of the gut microbiota to protect against simulated spaceflight-induced cardiac remodeling. The gut microbiota was transplanted from HU mice and from control mice into antibiotic-treated HU mice. The design of the FMT component of the study is shown in Figure 6A. Echocardiography was performed to monitor the structure and function of the heart after FMT. LVEF and LVFS were found to be significantly increased in mice that had been gavaged with the the CF group in comparison with the mice that had been gavaged with the the HF group (Figures 6B and 6C). Compared with the HF group, the LVPWd and LVPWs were significantly increased, LVIDd and LVVols were significantly decreased, and LVAWd, LVAWs, LVIDs, and LVVold were not significantly changed in the CF group (Figure S14). ANP, BNP, and MYH7 levels were significantly downregulated in the CF group when compared with those in the HF group (Figures 6D–6F). The serum TMAO concentration was lower in the CF group than in the HF group (Figure 6G), showed a negative correlation with LVEF (Figure 6H), and was positively correlated with the relative mRNA level of *ANP* (Figure 6I).

DISCUSSION

Spaceflight can have an adverse effect on the health of astronauts and a negative impact on the entire mission.[1,2] Recent research studies have shown that the human gut microbiota is profoundly affected by spaceflight.[5,6] The harsh environment of space, particularly weightlessness and radiation exposure, can have a negative effect on the structure and function of the cardiovascular system, and there is an increasing body of research showing how this system is affected by spaceflight and simulated spaceflight conditions in humans.[16,17] In view of the limited opportunities for spaceflight, we explored the effects of simulated spaceflight on cardiac remodeling by the gut microbiota in this study using HDBR macaque and HU mouse models. Our results demonstrate that the gut microbiota, fecal metabolites, and cardiac remodeling are markedly affected by HDBR in macaques and by HU in mice and that there is a correlation between cardiac remodeling and gut microbial-derived TMAO. FMT in our HU mouse model also demonstrated that cardiac remodeling is affected by the gut microbiota in both HU and control mice and that TMAO is correlated with cardiac remodeling. Previous studies have focused on the effects of simulated spaceflight on either cardiac remodeling or the gut microbiota,[24,25] and ours is the first to elucidate the impact of simulated spaceflight on cardiac remodeling by the gut microbiota. Our present findings are critical for research into how changes in the gut microbiota under spaceflight conditions affect physiological and psychological parameters in humans. Our results also provide insights into how an astronaut's gut microbiota might be maintained during spaceflight in a state that avoids adverse effects that have the potential to impede the success of the mission.

Previous research has shown that the composition and function of the gut microbiota fluctuates markedly after true or simulated spaceflight but recovers to a level similar to that before the flight.[5,6,25,26] Our present study found a gradual decrease in the Shannon index of the gut microbiota in macaques after HDBR and in mice after HU (Figures 1C and 5C), which is consistent with our previous study that involved true spaceflight. We found in our macaque model that the abundance of Bacteroidetes increased whereas that of Firmicutes decreased after HDBR (Figure 1D). Thus, the Firmicutes to Bacteroidetes (F/B) ratio was decreased, which is in line with our previous findings in true spaceflight and HDBR in humans. However, the F/B ratio in the gut microbiota was different in our mouse model from that in humans and macaques, with only a slight change in abundance after HU (Figure 5A). At the genus level, the abundance of *Bacteroides* increased and that of *Lactobacillus* decreased markedly in macaques after HDBR (Figure 1E). In the HU mouse model, the abundance of *Bacteroides* increased and that of *Lactobacillus* decreased markedly after HU, which was consistent with our results in the HDBR macaque model (Figure 5B). The increased abundance of *Bacteroides* after HDBR and HU was also consistent with our previous findings in true spaceflight and human HDBR, confirming that the abundance of *Bacteroides* is increased after spaceflight. *Bacteroides* is an efficient degrader of dietary fiber in the gut, where it generates propionate and phenolic acid, and is also an opportunistic pathogen that rapidly proliferates under stress conditions.[27–30] HDBR induced damage to the immune system in macaques, which was followed by an increase in the abundance of *Bacteroides* as an opportunistic pathogen. The decreased abundance of *Lactobacillus* after HDBR and HU was in line with our previous findings in true spaceflight, confirming that the abundance of *Lactobacillus* is decreased after spaceflight. *Lactobacillus* is a major producer of lactic acid in the gut, and several

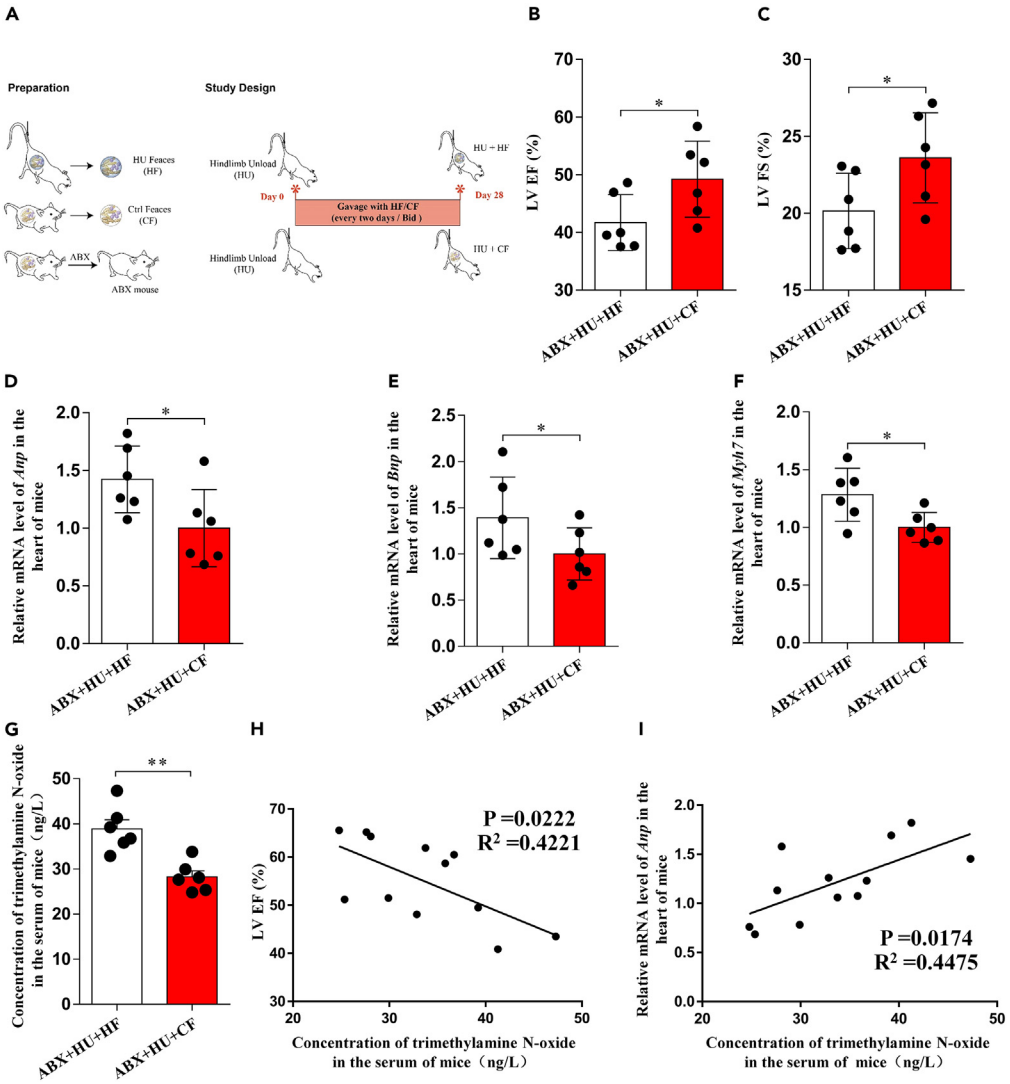

Figure 6. Cardiac remodeling in HU mice was influenced by the gut microbiota of HU and control mice and the correlation with serum TMAO concentration

(A) Overview of the study design and the protocol for fecal microbiota transplantation.

(B and C) Echocardiograms showing the LVEF and LVFS.

(D–F) Relative mRNA levels of *ANP*, *BNP*, and *MYH7* in the heart were analyzed by quantitative polymerase chain reaction assay.

(G) The serum TMAO concentration was detected by enzyme-linked immunosorbent assay.

(H) Correlation of LVEF with the serum TMAO concentration.

(I) Correlation of the relative mRNA level of *ANP* in the heart with the serum TMAO concentration.

*p < 0.05, **p < 0.01, and ***p < 0.001.

Lactobacillus taxa are known probiotics that can regulate the host immune system, enhance the metabolic capacity of the gut, and maintain balance in the gut microbiota.[31–33] Decreased abundance of *Lactobacillus* in the gut after HDBR could affect the functioning of the immune system and the balance of the gut microbiota in the macaque. The aforementioned results indicate that the HDBR macaque and HU mouse models have a good ability to simulate the effect of spaceflight on the gut microbiota. Combined with our previous work, some *Bacteroides* and *Lactobacillus* taxa can be defined as species biomarkers affected by true and simulated spaceflight.

In this study, we also found that fecal metabolites related to the purine metabolism pathway were markedly affected by HDBR in macaques (Figure 2B) and were reflected in serum (Figures S8B and S8D). The same fecal metabolites were also affected in the HU mouse model (Figures S13B and S13D). Other studies have confirmed that metabolites related to the purine metabolism pathway can modulate cardiac function.[34–36] Next, we detected the metabolites in the gut microbial TMAO pathway, SCFAs and bile acids, which are well known to be related to cardiac remodeling.[11,37,38] The metabolite content in the gut microbial TMAO pathway in macaques was increased after HDBR,

especially trimethylamine (Figures 2E–2I). However, there was no significant change in the SCFA or bile acid content (Figures S6 and S7). Therefore, we speculated that TMAO plays an important role in HDBR-induced cardiac remodeling in macaques and investigated their serum TMAO levels by enzyme-linked immunosorbent assay. We found an increase in the serum TMAO level after HDBR, which was correlated with cardiac remodeling (Figure 3). The same results were found in the HU mouse model (Figure 5). In this study, we used FMT to demonstrate the effect of the gut microbiota on simulated spaceflight-induced cardiac remodeling. We found that the gut microbiota could induce cardiac remodeling after HU in control mice and that there was a correlation with TMAO. Meanwhile, the gut microbiota in control mice could protect against cardiac remodeling in HU mice and, again, there was a correlation with TMAO (Figures 4 and 6). These results highlight the important role of the gut microbiota in simulated spaceflight-induced cardiac remodeling and suggest that maintaining the gut microbiota in astronauts during spaceflight is critical for avoidance of cardiac remodeling.

This is the first study to elucidate the impact of simulated spaceflight-induced changes in the gut microbiota on cardiac remodeling. These findings are critical for research into how changes in the gut microbiota affect the physiology and psychology of astronauts under spaceflight conditions. They also provide insights into how to maintain the gut microbiota in astronauts during spaceflight, which is critical for avoiding adverse effects and to the success of the spaceflight mission.

Limitations of the study

Because of the unique environmental conditions of spaceflight, we were unable to determine how specific factors, including simulated weightlessness, isolation, stress, and other factors, affect the gut microbiota. Another important question is whether the gut microbiota or cardiac remodeling is the major factor influenced by simulated spaceflight and whether each affects the other. In this study, we did not identify a specific species biomarker that affected cardiac function under simulated spaceflight conditions. Targeted preventive measures will be required to maintain cardiac performance during space missions, and the gut microbiota should be considered. More studies are warranted to identify specific species within the gut microbiota and the mechanism of spaceflight-induced cardiac remodeling under the unique environmental conditions of spaceflight.

STAR★METHODS

Detailed methods are provided in the online version of this paper and include the following:

- KEY RESOURCES TABLE
- RESOURCE AVAILABILITY
  - Lead contact
  - Materials availability
  - Data and code availability
- EXPERIMENTAL MODEL AND SUBJECT DETAILS
  - Animals
- METHOD DETAILS
  - Sampling
  - Fecal DNA extraction
  - Fecal 16S rRNA gene sequencing and data analyses
  - Fecal metagenomic sequencing and data analyses
  - Untargeted metabolomics and data analyses
  - Measurement of fecal TMA and related precursors
  - Measurement of fecal SCFAs
  - Measurement of fecal bile acids
  - Treatment with broad-spectrum antibiotics and FMT
  - Transthoracic echocardiography in macaques
  - Transthoracic echocardiography in mice
  - ELISA analysis
  - Quantitative RT-PCR
- QUANTIFICATION AND STATISTICAL ANALYSIS

SUPPLEMENTAL INFORMATION

Supplemental information can be found online at https://doi.org/10.1016/j.isci.2023.108556.

ACKNOWLEDGMENTS

This study was supported by National Natural Science Foundation of China Project (No. 82202073, 82192880, 82192882, and 82174203) and China Postdoctoral Science Foundation funded project (No. 2020M673670).

AUTHOR CONTRIBUTIONS

Z.L. and G.L. analyzed the data and wrote the manuscript. G.K. and X.H. contributed to samples collection. R.D., G.Z., W.X., Y.C., and W.S. played a key role in microbiome analyses. J.L., Yuheng Li, D.Z., X.Y., and X.J. provided critical feedback on data interpretation. Y.H., H.S., S.L., and Yingxian Li interpreted the data and designed the structure of the manuscript. All authors read and approved the final manuscript.

DECLARATION OF INTERESTS

The authors declare that they have no conflict of interest with the contents of this article.

INCLUSION AND DIVERSITY

We support inclusive, diverse, and equitable conduct of research.

Received: August 28, 2023
Revised: October 19, 2023
Accepted: November 20, 2023
Published: November 22, 2023

REFERENCES

1. Chapes, S.K. (2004). Lessons from Immune 1-3: what did we learn and what do we need to do in the future? J. Gravit. Physio.l *11*, P45–P48.
2. Zhang, L.F., and Hargens, A.R. (2018). Spaceflight-Induced Intracranial Hypertension and Visual Impairment: Pathophysiology and Countermeasures. Physiol. Rev. *98*, 59–87.
3. Lax, S., Smith, D.P., Hampton-Marcell, J., Owens, S.M., Handley, K.M., Scott, N.M., Gibbons, S.M., Larsen, P., Shogan, B.D., Weiss, S., et al. (2014). Longitudinal analysis of microbial interaction between humans and the indoor environment. Science *345*, 1048–1052.
4. Sun, J., Liao, X.P., D'Souza, A.W., Boolchandani, M., Li, S.H., Cheng, K., Luis Martinez, J., Li, L., Feng, Y.J., Fang, L.X., et al. (2020). Environmental remodeling of human gut microbiota and antibiotic resistome in livestock farms. Nat. Commun. *11*, 1427.
5. Garrett-Bakelman, F.E., Darshi, M., Green, S.J., Gur, R.C., Lin, L., Macias, B.R., McKenna, M.J., Meydan, C., Mishra, T., Nasrini, J., et al. (2019). The NASA Twins Study: A multidimensional analysis of a year-long human spaceflight. Science *364*, eaau8650.
6. Liu, Z., Luo, G., Du, R., Sun, W., Li, J., Lan, H., Chen, P., Yuan, X., Cao, D., Li, Y., et al. (2020). Effects of spaceflight on the composition and function of the human gut microbiota. Gut Microb. *11*, 807–819.
7. Schroeder, B.O., and Backhed, F. (2016). Signals from the gut microbiota to distant organs in physiology and disease. Nat. Med. *22*, 1079–1089.
8. Tang, T.W.H., Chen, H.C., Chen, C.Y., Yen, C.Y.T., Lin, C.J., Prajnamitra, R.P., Chen, L.L., Ruan, S.C., Lin, J.H., Lin, P.J., et al. (2019). Loss of Gut Microbiota Alters Immune System Composition and Cripples Postinfarction Cardiac Repair. Circulation *139*, 647–659.
9. Koh, A., De Vadder, F., Kovatcheva-Datchary, P., and Backhed, F. (2016). From Dietary Fiber to Host Physiology: Short-Chain Fatty Acids as Key Bacterial Metabolites. Cell *165*, 1332–1345.
10. Degnan, P.H., Taga, M.E., and Goodman, A.L. (2014). Vitamin B12 as a modulator of gut microbial ecology. Cell Metab. *20*, 769–778.
11. Wang, Z., Klipfell, E., Bennett, B.J., Koeth, R., Levison, B.S., Dugar, B., Feldstein, A.E., Britt, E.B., Fu, X., Chung, Y.M., et al. (2011). Gut flora metabolism of phosphatidylcholine promotes cardiovascular disease. Nature *472*, 57–63.
12. Ridler, C. (2016). Gut microbiota: D-amino acids employed against gut pathogens. Nat. Rev. Gastroenterol. Hepatol. *13*, 499.
13. Planer, J.D., Peng, Y., Kau, A.L., Blanton, L.V., Ndao, I.M., Tarr, P.I., Warner, B.B., and Gordon, J.I. (2016). Development of the gut microbiota and mucosal IgA responses in twins and gnotobiotic mice. Nature *534*, 263–266.
14. Tang, W.H., Wang, Z., Levison, B.S., Koeth, R.A., Britt, E.B., Fu, X., Wu, Y., and Hazen, S.L. (2013). Intestinal microbial metabolism of phosphatidylcholine and cardiovascular risk. N. Engl. J. Med. *368*, 1575–1584.
15. Tang, W.H.W., Li, D.Y., and Hazen, S.L. (2019). Dietary metabolism, the gut microbiome, and heart failure. Nat. Rev. Cardiol. *16*, 137–154.
16. MacNamara, J.P., Dias, K.A., Sarma, S., Lee, S.M.C., Martin, D., Romeijn, M., Zaha, V.G., and Levine, B.D. (2021). Cardiac Effects of Repeated Weightlessness During Extreme Duration Swimming Compared With Spaceflight. Circulation *143*, 1533–1535.
17. Scott, J.M., Stoudemire, J., Dolan, L., and Downs, M. (2022). Leveraging Spaceflight to Advance Cardiovascular Research on Earth. Circ. Res. *130*, 942–957.
18. Pavy-Le Traon, A., Heer, M., Narici, M.V., Rittweger, J., and Vernikos, J. (2007). From space to Earth: advances in human physiology from 20 years of bed rest studies (1986-2006). Eur. J. Appl. Physiol. *101*, 143–194.
19. Zhang, X., Chu, X., Chen, L., Fu, J., Wang, S., Song, J., Kan, G., Jiang, W., He, G., Chen, X., et al. (2019). Simulated weightlessness procedure, head-down bed rest impairs adult neurogenesis in the hippocampus of rhesus macaque. Mol. Brain *12*, 46.
20. Sonnenfeld, G. (2003). Animal models for the study of the effects of spaceflight on the immune system. Adv. Space Res. *32*, 1473–1476.
21. Shearer, W.T., Ochs, H.D., Lee, B.N., Cohen, E.N., Reuben, J.M., Cheng, I., Thompson, B., Butel, J.S., Blancher, A., Abbal, M., et al. (2009). Immune responses in adult female volunteers during the bed-rest model of spaceflight: antibodies and cytokines. J. Allergy Clin. Immunol. *123*, 900–905.
22. Kubo, K., Akima, H., Ushiyama, J., Tabata, I., Fukuoka, H., Kanehisa, H., and Fukunaga, T. (2004). Effects of 20 days of bed rest on the viscoelastic properties of tendon structures in lower limb muscles. Br. J. Sports Med. *38*, 324–330.
23. Perhonen, M.A., Zuckerman, J.H., and Levine, B.D. (2001). Deterioration of left ventricular chamber performance after bed rest : "cardiovascular deconditioning" or hypovolemia? Circulation *103*, 1851–1857.
24. Koenig, S.C., Ewert, D.L., Ludwig, D.A., Fanton, J.F., and Convertino, V.A. (2004). Bed rest affects ventricular and arterial elastances in monkeys: implications for humans. Aviat Space Environ. Med. *75*, 7–15.
25. Turroni, S., Rampelli, S., Biagi, E., Consolandi, C., Severgnini, M., Peano, C., Quercia, S., Soverini, M., Carbonero, F.G., Bianconi, G., et al. (2017). Temporal dynamics of the gut microbiota in people sharing a confined environment, a 520-day ground-based space simulation, MARS500. Microbiome *5*, 39.
26. Hao, Z., Li, L., Fu, Y., and Liu, H. (2018). The influence of bioregenerative life-support system dietary structure and lifestyle on the gut microbiota: a 105-day ground-based space simulation in Lunar Palace 1. Environ. Microbiol. *20*, 3643–3656.
27. Tremaroli, V., and Backhed, F. (2012). Functional interactions between the gut microbiota and host metabolism. Nature *489*, 242–249.
28. Russell, W.R., Duncan, S.H., Scobbie, L., Duncan, G., Cantlay, L., Calder, A.G., Anderson, S.E., and Flint, H.J. (2013). Major phenylpropanoid-derived metabolites in the human gut can arise from microbial fermentation of protein. Mol. Nutr. Food Res. *57*, 523–535.
29. Lee, S.M., Donaldson, G.P., Mikulski, Z., Boyajian, S., Ley, K., and Mazmanian, S.K. (2013). Bacterial colonization factors control specificity and stability of the gut microbiota. Nature *501*, 426–429.
30. Fischbach, M.A., and Sonnenburg, J.L. (2011). Eating for two: how metabolism establishes interspecies interactions in the gut. Cell Host Microbe *10*, 336–347.

31. Presti, I., D'Orazio, G., Labra, M., La Ferla, B., Mezzasalma, V., Bizzaro, G., Giardina, S., Michelotti, A., Tursi, F., Vassallo, M., et al. (2015). Evaluation of the probiotic properties of new Lactobacillus and Bifidobacterium strains and their *in vitro* effect. Appl. Microbiol. Biotechnol. *99*, 5613–5626.

32. Wang, C.Y., Chen, C.H., and Lai, C.C. (2022). Effect of Lactobacillus rhamnosus GG on Incident Pneumonia in Critically Ill Patients. JAMA *327*, 181–182.

33. Bender, M.J., McPherson, A.C., Phelps, C.M., Pandey, S.P., Laughlin, C.R., Shapira, J.H., Medina Sanchez, L., Rana, M., Richie, T.G., Mims, T.S., et al. (2023). Dietary tryptophan metabolite released by intratumoral Lactobacillus reuteri facilitates immune checkpoint inhibitor treatment. Cell *186*, 1846–1862.e6.

34. Zimmer, H.G. (1998). Significance of the 5-phosphoribosyl-1-pyrophosphate pool for cardiac purine and pyrimidine nucleotide synthesis: studies with ribose, adenine, inosine, and orotic acid in rats. Cardiovasc. Drugs Ther. *12* (*Suppl 2*), 179–187.

35. Manthei, S.A., Reiling, C.M., and Van Wylen, D.G. (1998). Dual cardiac microdialysis to assess drug-induced changes in interstitial purine metabolites: adenosine deaminase inhibition versus adenosine kinase inhibition. Cardiovasc. Res. *37*, 171–178.

36. Liu, Y., Yan, X., Mao, G., Fang, L., Zhao, B., Liu, Y., Tang, H., and Wang, N. (2013). Metabonomic profiling revealed an alteration in purine nucleotide metabolism associated with cardiac hypertrophy in rats treated with thiazolidinediones. J. Proteome Res. *12*, 5634–5641.

37. Marques, F.Z., Nelson, E., Chu, P.Y., Horlock, D., Fiedler, A., Ziemann, M., Tan, J.K., Kuruppu, S., Rajapakse, N.W., El-Osta, A., et al. (2017). High-Fiber Diet and Acetate Supplementation Change the Gut Microbiota and Prevent the Development of Hypertension and Heart Failure in Hypertensive Mice. Circulation *135*, 964–977.

38. Mayerhofer, C.C.K., Ueland, T., Broch, K., Vincent, R.P., Cross, G.F., Dahl, C.P., Aukrust, P., Gullestad, L., Hov, J.R., and Troseid, M. (2017). Increased Secondary/Primary Bile Acid Ratio in Chronic Heart Failure. J. Card. Fail. *23*, 666–671.

STAR★METHODS

KEY RESOURCES TABLE

REAGENT or RESOURCE	SOURCE	IDENTIFIER
Deposited data		
Raw data	the CNSA of CNGBdb: https://db.cngb.org/cnsa/	CNGBdb:CNP0004358
Oligonucleotides		
Rhesus macaque GAPDH forward:5′CGAGAGTCAGCCGCATTTTC-3′ reverse:5′GACTCCGACCTTCACCTTCC-3′	BGI	N/A
Rhesus macaque ANP forward:5′CCAACGCAGACCTGATGGAT-3′ reverse:5′GACTCCGACCTTCACCTTCC-3′	BGI	N/A
Rhesus macaque BNP forward:5′CGAGAGTCAGCCGCATTTTC-3′ reverse:5′GACTCCGACCTTCACCTTCC-3′	BGI	N/A
Rhesus macaque MYH7 forward:5′CGAGAGTCAGCCGCATTTTC-3′ reverse:5′GACTCCGACCTTCACCTTCC-3′	BGI	N/A
Mouse Gapdh forward:5′AACATCAAATGGGGTGAGGCC-3′ reverse:5′GTTGTCATGGATGACCTTGGC-3′	BGI	N/A
Mouse Anp forward:5′TTCGGGGGTAGGATTGACAG-3′ reverse:5′CACACCACAAGGGCTTAGGA-3′	BGI	N/A
Mouse Bnp forward:5′TGTTTCTGCTTTTCCTTTATCTG-3 reverse:5′TCTTTTTGGGTGTTCTTTTGTGA-3′	BGI	N/A
Mouse Myh7 forward:5′CCCCTTCCTGCGAAAATCTG-3′ reverse:5′TCTTTTTGGGTGTTCTTTTGTGA-3′	BGI	N/A
Software and algorithms		
FLASH (V1.2.7)	N/A	http://ccb.jhu.edu/software/FLASH/
QIIME 2 (V2020.11)	N/A	https://qiime2.org/
UCHIME algorithm	N/A	http://www.drive5.com/usearch/manual/uchime_algo.html
Silva database	N/A	https://www.arb-silva.de/
Uparse (v7.0.1001)	N/A	http://drive5.com/uparse/
MUSCLE (Version 3.8.31)	N/A	http://www.drive5.com/muscle/
Readfq (V8)	N/A	https://github.com/cjfields/readfq
SOAPdenovo (V2.04)	N/A	http://soap.genomics.org.cn/soapdenovo.html
MetaGeneMark (V2.10)	N/A	http://topaz.gatech.edu/GeneMark/
CD-HIT (V4.5.8)	N/A	http://www.bioinformatics
SoapAligner (soap2.21)	N/A	http://soap.genomics.org.cn/soapaligner.html
NR database (V20161115)	N/A	https://www.ncbi.nlm.nih.gov/
DIAMOND (V0.7.9)	N/A	https://github.com/bbuchfink/diamond/

(*Continued on next page*)

Continued

REAGENT or RESOURCE	SOURCE	IDENTIFIER
KEGG (V201609)	N/A	http://www.kegg.jp/kegg/
eggnog (V4.5)	N/A	http://eggnogdb.embl.de/#/app/home
CAZy (V20150704)	N/A	http://www.cazy.org/

RESOURCE AVAILABILITY

Lead contact

Further information and requests for resources should be directed to and will be fulfilled by the lead contact, Zizhong Liu (liuzizhong911@163.com).

Materials availability

This study did not generate new unique reagents.

Data and code availability

- Raw data have been deposited at the CNSA of CNGBdb and are publicly available as of the date of publication. The DOI and accession number are listed in the key resources table. All other data reported in this paper will be shared by the lead contact upon request.
- This paper does not report original code.
- Any additional information required to reanalyze the data reported in this paper is available from the lead contact upon request.

EXPERIMENTAL MODEL AND SUBJECT DETAILS

Animals

Nine healthy male rhesus macaques (age 5–7 years; weight 9–10 kg) were randomly allocated to an HDBR group (n=6) or a control group (n=3). All macaques were treated strictly according to the National Standard (GB14922.2–2001) on a 12-h light/dark cycle with the temperature controlled at 23°C and free access to food and water. All the macaques received 3 months of domestication at the China Astronaut Research and Training Center before the HDBR experiment. The HDBR macaques were subjected to 10 degrees of head-down bed rest while wearing a confinement jacket. The control macaques were housed singly in cages that were large enough to allow them to move freely. After 42 days of the HDBR or control experiment, all macaques were anesthetized by intramuscular injection of ketamine 10 mg/kg and euthanized by exsanguination followed by immediate collection of serum and the heart.

Eight-week-old male C57BL/6J mice were used in this study. They were bred and maintained in the SPF Animal Research Building at the China Astronaut Research and Training Center on a 12-h light/dark cycle with the temperature controlled at 23°C and free access to food and water. The mice were fed on a standard maintenance murine diet. The mice were euthanized after 4 weeks of HU by injection with 2.5% 2,2,2-tribromoethanol (Avertin; Sigma-Aldrich, St Louis, MO, USA), after which the serum and heart were collected immediately.

All experimental procedures involving the macaques were approved by the China Astronaut Research and Training Center ethics committee (reference number ACC-IACUC-2019-002). All experimental procedures involving the mice were approved by the Animal Care and Use Committee of the China Astronaut Research and Training Center. All animal studies were performed in accordance with the approved guidelines for the use and care of live animals.

METHOD DETAILS

Sampling

Fecal samples of all rhesus macaques were collected at eight time-points, including one weeks before HDBR (B7), one day before HDBR (B1), one week during HDBR (D7), two weeks during HDBR (D14), three weeks during HDBR (D21), four weeks during HDBR (D28), five weeks during HDBR (D35) and six weeks during HDBR (D42). Serum samples of all rhesus macaques were collected at four time-points, including one day before HDBR (B1), two weeks during HDBR (D14), four weeks during HDBR (D28) and six weeks during HDBR (D42). All fecal, serum and heart samples of rhesus macaques were collected in sterile vials and immediately transferred to a −80°C freezer. Fecal samples of mice which used to analyze the composition of gut microbiota were collected at eight time-points, including one day before HU (B1), one week during HU (D7), two weeks during HU (D14), three weeks during HU (D21), four weeks during HU (D28), one week after recovery (R7), two weeks after recovery (R14) (D35) and four weeks after recovery (R28). All fecal, serum and heart samples of mice were collected in sterile vials and immediately transferred to a −80°C freezer.

Fecal DNA extraction

Rhesus macaques and mice stool samples (180–220mg) were weighed in 2 ml microcentrifuge tubes and placed on ice. Total DNA from fecal microbiotas was extracted using the QIAamp Fast DNA Stool Mini Kit (QIAGEN, Germany) per the manufacturer's instructions (see the

QIAamp Fast DNA Stool Mini Kit Handbook, www.qiagen.com/handbooks). Degradation degree and potential contamination of the DNA were analyzed using 1% agarose gels. DNA purity was determined using the NanoPhotometer® Spectrophotometer (IMPLEN, CA, USA), and the DNA concentration was measured using the Qubit® dsDNA Assay Kit in Qubit® 2.0 Fluorometer (Life Technologies, CA, USA).

Fecal 16S rRNA gene sequencing and data analyses

Fecal DNA was diluted to 1ng/μL using sterile water according to the concentration. 16S rRNA genes of distinct regions(16SV3-V4) were amplified used specific primer with the barcode. The PCR products was purified with Qiagen Gel Extraction Kit (Qiagen, Germany). TruSeq® DNA PCR-Free Sample Preparation Kit (Illumina, USA) was used to generate Sequencing libraries following manufacturer's recommendations and index codes were added. Qubit@ 2.0 Fluorometer (Thermo Scientific) and Agilent Bioanalyzer 2100 system were used to assess the library quality. The libraries were sequenced on an Illumina NovaSeq platform and 250 bp paired-end reads were generated. FLASH was used to merge paired-end reads, and the splicing sequences were called raw tags. According to the QIIME 2quality controlled process, the raw tags were performed to obtain the clean tags. The UCHIME algorithmwas used to compared the clean tags with the reference database(Silva database,) and to obtain the effective tags. Uparse software was used to perform sequences, and the sequences with ≥97% similarity were assigned to the same OTUs. Taxonomic information was annotate by the Silva Database, and the MUSCLE software was used to study phylogenetic relationship. OTUs abundance information were normalized by the sample with the least sequences. All alpha diversity indices were calculated with QIIME 2(Version 2020.11) and displayed with R software (Version 2.15.3). QIIME 2 software (Version 2020.11) was used to calculate the beta diversity on both weighted and unweighted Unifrac.

Fecal metagenomic sequencing and data analyses

One microgram of qualified DNA was used to construct the library. DNA samples were fragmented to 350 bp by sonication, then the DNA fragments were end-polished, A-tailed, and ligated with the full-length adaptor for Illumina sequencing with further PCR amplification. Libraries were analyzed for size distribution using the Agilent2100 Bioanalyzer (Agilent, USA) and quantified via real-time PCR. The libraries were sequenced on an Illumina HiSeq platform.

Raw data obtained from the Illumina HiSeq sequencing platform were preprocessed by Readfq, and the acquired clean data were used for subsequent analysis. The clean data were analyzed using SOAPdenovo software, and the Scaftigs were obtained. All the sample details of the quality of their assemblies were present in Table S2. The Scaftigs (≥ 500 bp) were used to predict the open reading frame (ORF) using MetaGeneMark and CD-HIT software. The website, org/cd-hit, was used to obtain the initial gene catalog from the predicted ORF. Clean data from each sample were mapped to the initial gene catalog using SoapAligner software. The obtained gene catalog (Unigenes) was eventually used for subsequent analyses. The obtained Unigenes were used to blast the sequences for the bacteria, fungi, archaea and viruses, which were extracted from the NR database of NCBI using DIAMOND software. We used the lowest common ancestor (LCA) algorithm to obtain the number of genes and abundance information for each sample in each taxonomic hierarchy (kingdom, phylum, class, order, family, genus, and species). DIAMOND software (V0.7.9) was used to blast Unigenes to functional databases, including the KEGG, eggnog and CAZy databases, for the blast results, and the best blast hit was used for subsequent analysis.

Untargeted metabolomics and data analyses

Stool samples (100 mg) from each macaque and mouse were ground with liquid nitrogen, after which the homogenate was resuspended in prechilled 80% methanol and 0.1% formic acid (FA) using a vortex mixer. Serum samples (100 μL) from the macaques were placed in EP tubes and resuspended in prechilled 80% methanol and 0.1% FA using a vortex mixer. The samples were incubated on ice for 5 min and then centrifuged at 15,000 g for 20 min at 4°C, using LC-MS-grade water to dilute the supernatant to a final concentration containing 53% methanol. Next, the samples were transferred to new tubes and centrifuged at 15,000 g for 20 min at 4°C, after which the supernatant was injected into a high-performance liquid chromatography tandem mass spectrometry (LC-MS/MS) system for analysis. The raw data files generated by UHPLC-MS/MS were processed using Compound Discoverer 3.1 (ThermoFisher Scientific, Waltham, MA, USA) for peak alignment, peak picking, and quantitation of each metabolite. Peak intensities were normalized to total spectral intensity and matched with the mzCloud (https://www.mzcloud.org/), mzVault, and MassList databases to obtain accurate qualitative and relative quantitative results. All statistical analyses were performed using R version 3.4.3, Python version 2.7.6, and CentOS release 6.6. When data were not normally distributed, normal transformations were attempted using the area normalization method.

Measurement of fecal TMA and related precursors

Fecal trimethylamine and related precursors, including betaine, creatinine, L-carnitine, and choline hydroxide, were quantified by LC-MS/MS. In this study, an Acquity UPLC I-Class (Waters, Milford, MA, USA) + QTRAP 6500+ (Sciex, Framingham, MA, USA) was used as the analytical instrument and MultiQuant software (Sciex) was used for automatic identification and integration of each multi-reaction monitoring (MRM) transition (ion pair). Liquid chromatography was performed using a Waters BEH HILIC column (100 mm × 2.1 mm, 1.7 um) with a mobile phase A of ultrapure water + 0.15% FA + 10 mM ammonium formate and a mobile phase B of acetonitrile.

Measurement of fecal SCFAs

Fecal SCFAs were quantified by LC-MS/MS. The Waters Iclass-AB + Sciex 6500 system was used as the analytical instrument and MultiQuant software was used for automatic identification and integration of each MRM transition (ion pair). Liquid chromatography was performed using a Waters BEH C18 column (model, 1.7 μm × 2.1 mm × 100 mm) with a mobile phase A of H_2O + 0.1% FA and a mobile phase B of ACN + 0.1% FA.

Measurement of fecal bile acids

Fecal bile acids were quantified by LC-MS/MS. A liquid-mass spectrometry system consisting of an Acquity UPLC I-Class system (Waters) and a Triple Quad 6500+ mass spectrometer (Sciex) was used as the analytical instrument and MultiQuant software was used for automatic identification and integration of each MRM transition (ion pair). Liquid chromatography was performed using a Waters Acquity UPLC BEH C18 column (2.1 mm × 100 mm, 130 Å, 1.7 μm) with a mobile phase A of water + 5 mM ammonium acetate + 0.01% FA and a mobile phase B of 70% acetonitrile + 30% methanol + 0.01% FA.

Treatment with broad-spectrum antibiotics and FMT

Antibiotic-treated mice were supplied with autoclaved water supplemented with antibiotics (ampicillin 1 g/L, gentamicin 1 g/L, metronidazole 1 g/L, neomycin 1 g/L, and vancomycin 0.5 g/L) for 2 weeks. Two fresh fecal pellets from a control mouse and an HU mouse were homogenized in 1 mL of phosphate-buffered saline and passed through a 100-mm filter, after which each mouse was administered 200 μL of the resulting suspension by oral gavage.

Transthoracic echocardiography in macaques

The macaques were anaesthetized using ketamine hydrochloride (Shanghai Zhongxi Pharmaceutical Co., Ltd, Shanghai, China) at a dosage of 10 mg/kg administered intramuscularly and placed in the dorsal decubitus position. The examination was conducted only when the animal was in a stable sedated state. Two-dimensional M-mode echocardiography was performed using an IE33 ultrasound system (Philips Healthcare, Andover, MA, USA). All measurements and calculations were from 3–5 consecutive cardiac cycles and made in real time during examination with the aid of the computer software. Averaged posterior LV wall thickness, interventricular septal thickness, internal dimensions at diastole and systole (LVIDd and LVIDs, respectively), end-diastolic left ventricular volume, end-systolic left ventricular volume, LVEF, and LVFS were measured.

Transthoracic echocardiography in mice

Mice were lightly anesthetized with 2,2,2-tribromoethanol (0.2 ml/10 g body weight of a 1.2% solution), two dimensional (2D) guided M-mode echocardiography was performed using a high resolution imaging system (Vevo 770, Visual-Sonics Inc., Toronto, ON, Canada). Two-dimensional images are recorded in parasternal long- and short-axis projections with guided M-mode recordings at the midventricular level in both views. Left ventricular (LV) cavity size and wall thickness are measured in at least three beats from each projection. Averaged LV wall thickness [interventricular septum (IVS) and posterior wall (PW) thickness] and internal dimensions at diastole and systole (LVIDd and LVIDs, respectively) are measured. LV fractionalshortening ((LVIDd – LVIDs)/LVIDd), relative wall thickness [(IVS thickness + PW thickness)/LVIDd], and LV mass [LV Mass = 1.053 × [(LVIDd + LVPWd + IVSd)3 – LVIDd3]] are calculated from the M-mode measurements. LV ejection fraction (EF) was calculated from the LV cross-sectional area (2-D short-axis view) using the equation LV %EF = (LV Vold – LV Vols)/LV Vold × 100%.

ELISA analysis

Serum of rhesus macaques and mice was collected to detect the concentration of TMAO and stored at –80°C until use for the ELISA analysis. The ELISA was performed by conventional colorimetric detection using an ELISA kit according to the manufacturer's instructions. In brief, 50 ml aliquots of serum were pipetted in duplicate into the wells of the precoated ELISA plate. Then, 50 ml of antibody solution was added to each well. The plates were then incubated at 37°C for 30 min on a shaking device. After incubation, the plates were washed three times with washing buffer.

Quantitative RT-PCR

The total RNA from hearts of rhesus macaques and mice were extracted with TRIzol reagent (Invitrogen) according to the manufacturer's instructions. RNA (0.5μg) was reverse transcribed with PrimeScript RT reagent Kit(TaKaRa, Dalian, China) according to the manufacturer's instructions. Two microlitres of cDNA were used for detecting mRNA expression by quantitative PCR (qPCR) using a SYBR Premix ExTaq II Kit (TaKaRa). GAPDH of rhesus macaques and Gapdh of mice were used as a normalization control for mRNA measurements.

QUANTIFICATION AND STATISTICAL ANALYSIS

Data are presented as mean ± standard deviation (SD). One-way ANOVA was used to assess between-group differences, Graphpad Prism version 7.0c was used to follow by post-hoc pairwise repetitive comparisons with Turkey test.